Electrostatic Mutations in Iberiotoxin as a Unique Tool for Probing the Electrostatic Structure of the Maxi-K Channel Outer Vestibule†

Theodore J. Mullmann,‡ Petraki Munujos,§ Maria L. Garcia,§ and Kathleen M. Giangiacomo*,‡

Department of Biochemistry, Temple University School of Medicine, 3420 North Broad Street, Philadelphia, Pennsylvania 19140, and Department of Membrane Biochemistry and Biophysics, Merck Research Laboratories, P.O. Box 2000, Rahway, New Jersey 07065

Received August 24, 1998; Revised Manuscript Received December 17, 1998

ABSTRACT: Iberiotoxin (IbTX or α-KTx 1.3), a selective, high-affinity blocker of the large-conductance, calcium-activated (maxi-K) channel, exhibits a unique, asymmetric distribution of charge. To test how these charges control kinetics of IbTX binding, we generated five mutants at two positions, K27 and R34, that are highly conserved among other isotoxins. The dissociation and association rate constants, k_{off} and k_{on}, were determined from toxin-blocked and -unblocked durations of single maxi-K channels incorporated into planar lipid bilayers. Equilibrium dissociation constant (K_d) values were calculated from k_{off}/k_{on}. The IbTX mutants K27N, K27Q, and R34N caused large increases in K_d values compared to wild-type, suggesting that the IbTX interaction surface encompasses these residues. A well-established pore-blocking mechanism for IbTX predicts a voltage dependence of toxin-blocked times following occupancy of a potassium binding site in the channel pore. Time constants for block by K27R were ∼5-fold slower at −20 mV versus +40 mV, while neutralization of K27 relieved the voltage dependence of block. This suggests that K27 in IbTX interacts with a potassium binding site in the pore. Neutralized mutants of K27 and R34, with zero net charge, displayed toxin association rate constants ∼10-fold slower than wild-type. Association rates for R34N diminished ∼19-fold when external potassium was increased from 30 to 300 mM. These findings suggest that simple net charge and diffusional processes do not control ingress of IbTX into the channel vestibule.

The α-K channel toxins (α-KTx)[1] from the venoms of scorpions are highly basic peptides that bind to potassium channels with high affinity to block the flow of K^+ ions through the channel pore (*1*−*3*). A well-founded model for toxin block of current through potassium channels suggests a simple bimolecular plugging mechanism in the extracellular vestibule of the channel pore. This model is based on detailed kinetic studies of IbTX (*4*) and charybdotoxin (ChTX or α-KTx 1.1) (*5*, *6*) block of single, large-conductance, calcium-activated potassium (maxi-K) channels incorporated into planar lipid bilayers and of ChTX block of macroscopic current through the voltage-gated Shaker potassium channel (*7*). The location of the toxin binding site in the extracellular pore has guided efforts to identify the pore region of the voltage-gated *Shaker* potassium channel (*8*−*10*) and to map a low-resolution image of the maxi-K (*11*, *12*) and *Shaker* (*13*, *14*) channel external vestibules. Thus, the α-K toxins are powerful tools for probing the structure of the potassium channel vestibules and the structures which underlie permeation in potassium channels.

The electrostatic potential around the channel vestibule may play an important role in defining permeation, and hence rates of ion flux, through a channel. The maxi-K channel is unique because it allows K^+ ions to diffuse at rates ∼10-fold faster than those observed for all other potassium channels. Despite this high ionic flux, the maxi-K channel maintains high selectivity for K^+ over Na^+. Electrostatic calculations revealed that this apparent paradox, of rapid ionic flux and ion selectivity, can be explained by placing unique fixed charges in the vestibule close to the selectivity filter in the pore (*15*). Thus, the uncommon high-conductance properties of the maxi-K channel may be explained by unique electrostatic features of its vestibule that are distinct from other potassium channel vestibules.

Among the α-K toxin subfamilies there appears to be a gross level of specificity for the maxi-K over voltage-gated potassium (Kv) channels (*2*, *3*). Subfamilies 2.x and 3.x block many Kv channels with high affinity but not the maxi-K channel. In contrast, peptide toxins assigned to the α-KTx 1.x subfamily exhibit high-affinity interactions with the maxi-K channels. Furthermore, two of the toxins in subfamily 1.x, IbTX (α-KTx 1.3) and limbatus toxin (LbTX or α-KTx 1.4), appear to be highly selective for the maxi-K channel

† This work was supported in part by NIH Grant GM52179 (to T.J.M. and K.M.G.).

* To whom reprint requests should be addressed.

‡ Temple University School of Medicine.

§ Merck Research Laboratories.

[1] Abbreviations: α-KTx, potassium channel toxin; α-KTx 1.1, charybdotoxin; α-KTx 1.3, iberiotoxin; α-KTx 1.4, limbatus toxin; α-KTx 3.2, agitoxin2; ChTX, charybdotoxin; DH, Debye−Huckel; IbTX, iberiotoxin; K_d, equilibrium dissociation constant; k_{off}, dissociation rate constant; k_{on}, second-order association rate constant; K_v channel, voltage-gated potassium channel; LbTX, limbatus toxin; maxi-K channel, large-conductance, calcium-activated potassium channel.

10.1021/bi982040+ CCC: $18.00
Published on Web 02/05/1999

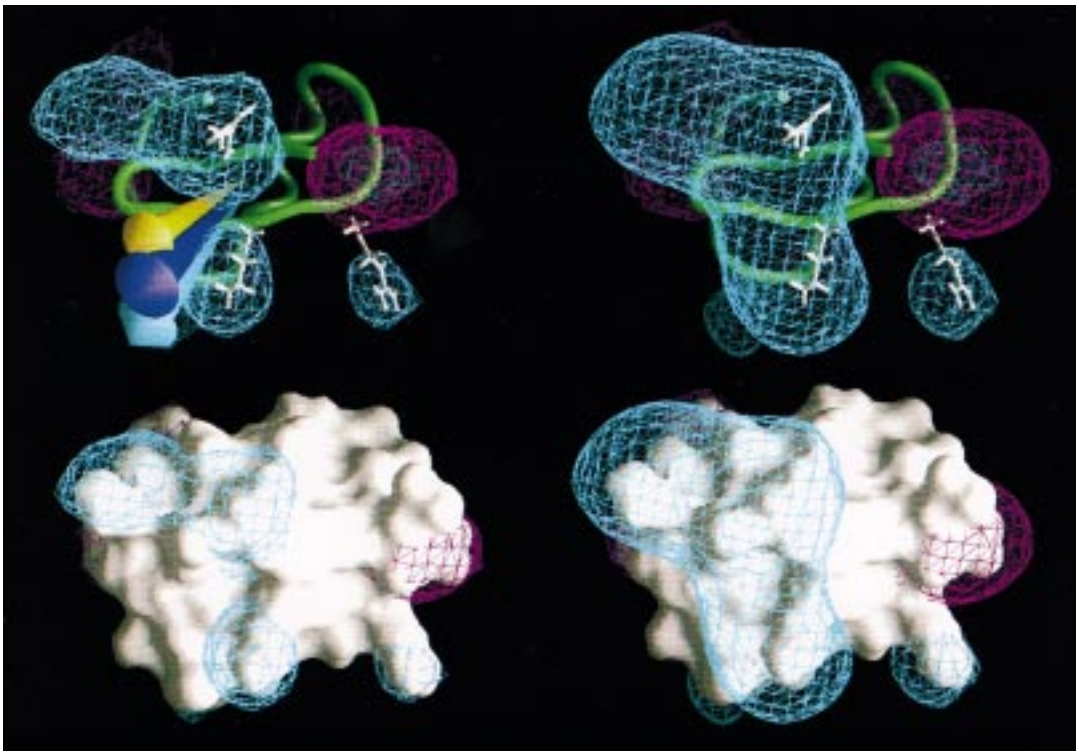

FIGURE 1: Isopotential energy surfaces and molecular surfaces for IbTX. (Left side) Isopotential energy surfaces at 3 kT (turquoise) and −3 kT (magenta) are shown overlaying the α-carbon backbone (top) and the molecular surface (bottom). The calculated dipole moments for wild-type IbTX and neutralized mutants of K27 and R34 are shown in blue, yellow, and turquoise, respectively. The side chain bonds for R25, K27, and R34 are shown in white. (Right side) Isopotential energy surfaces at 2 kT (turquoise) and −2 kT (magenta) are shown overlaying the α-carbon backbone (top) and the molecular surface (bottom). Electrostatic calculations for the structures shown were done using GRASP (*26*) with a charge set that includes only the terminal nitrogen and oxygen atoms of lysine, arginine, aspartate, and glutamate residues and the N- and C-terminal atoms. The salt concentration was 15 mM. When the partial charges of the α-carbon backbone were included in these calculations, the volume enclosed by these isopotential energy surfaces increased slightly. However, an overlay of these isopotential contour surfaces with the molecular surface was almost indistinguishable from those shown.

(*16*−*18*). Thus, IbTX and LbTX may serve as tools for probing unique features of the maxi-K channel vestibule.

A unique feature of IbTX and LbTX is that they contain many acidic residues. For IbTX, the almost equal number of basic (7) and acidic (6) residues translates into an asymmetric distribution of charge which can be quantitatively described by the toxin dipole moment (μ = 235 D). This charge asymmetry can also be seen from plots of positive (2 and 3 kT) and negative (−2 and −3 kT) isopotential energy surfaces for IbTX shown in Figure 1. From these isopotential plots, it is clear that most of the positive electrostatic potential resides around the β-sheet face while the negative electrostatic potential is located near the back, helix face of the molecule. Scanning mutagenesis studies of ChTX (α-KTx 1.1) (*11, 12, 14*) and agitoxin 2 (AgTX2 or α-KTx 3.2) (*19, 20*) showed that residues emanating from the β-sheet face form the α-KTx receptor surface. Thus, α-KTx residues around the β-sheet face likely interact with the external potassium channel vestibule.

The unique charge asymmetry observed for IbTX may underlie some of its ability to discriminate the maxi-K channel from other Kv channels. More fundamentally, the unique electrostatic structure of IbTX may provide insight into novel electrostatic features of the maxi-K channel vestibule. To begin to explore the electrostatic structure of the maxi-K channel vestibule, we examine the effects of the electrostatic IbTX mutants K27N, K27Q, K27R, R34N, and R34D on block of single maxi-K channels incorporated into planar lipid bilayers.

MATERIALS AND METHODS

Materials. Sarcolemmal membranes were purified from bovine aortic smooth muscle as described previously (*21*). "Restriction Protease Factor Xa" was obtained from Boerhinger Mannheim (Mannheim, Germany); Ni^{2+}-NTA agarose was from Qiagen (Santa Clarita, CA); T4 DNA polymerase and T4 DNA ligase were from BioRad (Richmond, CA); Taq DNA polymerase was from Perkin-Elmer; nucleotide triphosphates were from Pharmacia Biotech (Piscataway, NJ); and restriction enzymes were from Promega (Madison, WI).

Polystyrene cuvettes for bilayer experiments contained a 150 micron aperture and were purchased from Warner Instruments, Inc. (Hamden, CT). 1-Palmitoyl-2-oleoylphosphatidylethanolamine (POPE) and 1-palmitoyl-2-oleoylphosphatidylcholine (POPC) were purchased from Avanti Polar Lipids, Inc. (Birmingham, AL). Decane from Fisher Scientific, Inc. (Springfield, NJ) was 99.9% mole purity. All other reagents were of the highest purity commercially available.

Construction of the Synthetic IbTX Gene and Site-Directed Mutants. The plasmid pG9IbTX, encoding six histidine residues between the fusion protein and the factor Xa cleavage site, and the wild-type IbTX sequence was constructed as described (*22*). IbTX mutations were generated using a two-step polymerase chain reaction point mutagenesis strategy. Plasmids containing the IbTX gene and site-directed mutants were propagated using the *Escherichia coli* strain DH5 α. The identity of all DNA constructs was verified using dideoxy sequencing.

Purification of rIbTX Mutant Peptides. E. coli strain BL21-(DE3) harboring the IbTX plasmids were cultured and induced with isopropyl-1-thio-β-D-galactopyranoside as previously described (*23*). Purification of the T7 gene 9-IbTX fusion protein and cleavage of the rIbTX peptides from the fusion protein were as described (*22*). rIbTX peptides with a net charge of +1 were purified by mono-S cation exchange chromatography as described (*22*). IbTX mutants with a net charge of 0 were loaded onto a mono-S column (HR 10/10 Pharmacia Biotechnology Inc.) equilibrated at pH 7.0 with 20 mM sodium borate. The IbTX mutant R34D, with a net charge of −1, was loaded onto a mono-Q anion exchange column equilibrated with 20 mM Tris-HCl, pH 9.0, and eluted with a linear gradient of NaCl in equilibration buffer.

The N-terminal glutamine was cyclized to pyroglutamine, by incubating IbTX peptides in the presence of 5% acetic acid for 16 h at 45 °C. Under these conditions, rIbTX mutants were at least 80−90% cyclized as determined by the yields of the first 4−5 residues after Edman degradation. Higher incubation temperatures, to achieve complete cyclization, caused extensive hydrolysis of rIbTX peptides with consequently lower yields. Final purification of the peptides was achieved by reverse-phase HPLC as described (*16*). For R34 mutations in IbTX, the cyclized and uncyclized forms of the peptides were easily separable by HPLC. The identity of all peptides was verified by Edman degradation before cyclization and by amino acid hydrolysis.

Binding Studies. Binding of ^{125}I-ChTX to bovine aortic sarcolemmal membranes was done as described (*16*). Native IbTX and the mutants K27R, K27N, K27Q, R34N, and R34D inhibited binding with K_i values of 0.4, 3.4, 32, ≫30, 209, and ≫300 nM, respectively.

Recordings of Maxi-K Channels in Planar Lipid Bilayers. Planar lipid bilayers were formed and maxi-K channels from bovine aortic sarcolemmal membranes were fused with the bilayer as described previously (*4*). The lipids were composed of a 7:3 molar ratio of POPE/POPC. The exact compositions of the solutions are described in the figure legends.

Currents through single maxi-K channels were detected and amplified using a Dagan 3900A integrating patch clamp amplifier (Dagan Corp.) as described (*4*). Single channel currents were recorded onto a video cassette tape with a VR10B digital data recorder (Instrutech, Inc.) and were digitally encoded with Pulse (HEKA Electronik, Inc.) onto a HD DAT 2.2 tape drive (Intuitive Systems, Inc.) which was mounted onto a Macintosh computer. In addition, for IbTX mutants with slow blocking kinetics, single channel recordings were played onto a Dash IV model XL chart recorder (Astro Med., Inc) and blocked times were measured directly from the chart paper.

The single channel records were refiltered off-line on a Macintosh computer using a digital Guassian filter in TAC (SKALAR Instruments, Inc.) and events were detected using a threshold detection algorithm in TAC. The distributions of closed and open times were plotted and fitted as sums of exponential components using TACfit (SKALAR Instruments, Inc.).

Toxin-blocked times were distinguished from closed times as described (*4*). The toxin dissociation rate constant (k_{off}) and pseudo-first-order toxin association rate constant (k_{on}[toxin]) values were calculated from the average toxin-blocked (T_{block}) and -unblocked times ($T_{unblock}$), respectively, as shown in eqs 1 and 2.

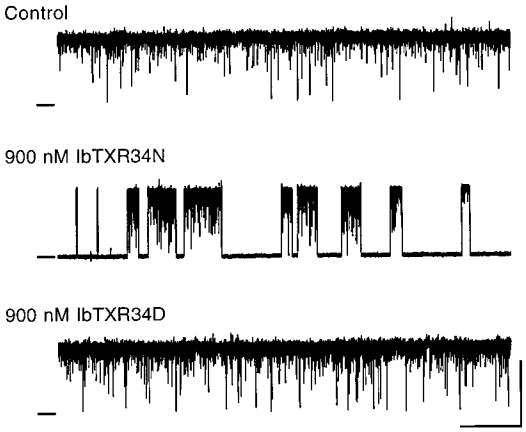

FIGURE 2: Effects of R34 mutations in IbTX on current through single maxi-K channels. Currents through single maxi-K channels from bovine aortic smooth muscle incorporated into planar lipid bilayers are shown in the absence and presence of the IbTX mutants R34N and R34D. The closed current level is indicated by the lines to the left. The indicated time and current scale bars represent 30 s and 10 pA, respectively. Currents were filtered at 200 Hz for display. Conditions: 150 mM KCl; 10 mM Hepes, pH 7.2, inside and outside; 305 μM $CaCl_2$ inside; 60 μg/mL BSA outside; and +40 mV.

$$k_{off} = 1/T_{block} \quad (1)$$

$$k_{on}[\text{toxin}] = 1/T_{unblock} \quad (2)$$

In this work, mean blocked and unblocked times were each calculated from an average of 118 events. The toxin equilibrium dissociation constant (K_d), values were calculated from the second-order toxin association rate constant, k_{on}, and k_{off} values as shown in eq 3.

$$K_d = k_{off}/k_{on} \quad (3)$$

Electrostatic Calculations. The electrostatic potential throughout the volume of the toxin was calculated using the atomic coordinates of the three-dimensional structure for IbTX (*24*) using the program GRASP as described (*25, 26*). The electrostatic potential calculations were done using two different charge sets. One includes only the ionizable nitrogens and oxygens at the N and C termini and on the lysine, arginine, aspartate, and glutamate residues. The other charge set assigns partial charges to all ionizable residues and to atoms in the α-carbon backbone.

RESULTS

K27 and R34 Form Part of the IbTX Receptor Surface for the Maxi-K Channel Vestibule. Figures 2 and 3 show the effects of R34 and K27 IbTX mutants on currents through single maxi-K channels. While 900 nM IbTX R34D had no apparent effect on channel activity, all other mutant toxins caused the appearance of nonconducting silent periods, seconds in duration, interrupted by periods of normal channel activity. Kinetic studies with wild-type IbTX showed that these silent periods represent times when toxin is bound to the channel and therefore are inversely related to the toxin dissociation rate constant (*4*). The mean blocked times for K27R, K27N, K27Q, and R34N averaged from several

Table 1: Toxin Blocking Kinetics from Single-Maxi K Channels[a]

mutant	V_m (mV)	K_d (nM)	k_{on} ($\times 10^6$ M^{-1} s^{-1})	k_{off} (s^{-1})
IbTX	+40	1.7 ± 0.5[b]	1.2 ± 0.1[b]	0.002 ± 0.0006[b]
IbTX K27R	+40	6.8 ± 0.9	1.4 ± 0.19	0.0094 ± 0.0006
	−20	2.07 ± 0.48	0.957 ± 0.063	0.002 ± 0.0006
IbTX K27N	+40	32 ± 15	0.19 ± 0.05	0.0046 ± 0.0009
	−20	11.6 ± 1.37	0.465 ± 0.0487	0.0053 ± 0.00007
IbTX K27Q	+40	1380 ± 159	0.06 ± 0.01	0.09 ± 0.02
	−20	1610 ± 424	0.147 ± 0.0734	0.21 ± 0.06
IbTX R34N	+40	600 ± 130	0.11 ± 0.02	0.066 ± 0.019
	−20	139 ± 21	0.269 ± 0.0825	0.033 ± 0.004
IbTX R34D	+40	≫17000		

[a] The first-order dissociation rate constants, k_{off}, and the second-order association rate constants, k_{on}, were determined from average toxin blocked and unlocked times, respectively, as described in Material and Methods. Each value was the average of two to nine separate measurements; error bars represent standard errors of the mean. Experimental conditions were as described in Figure 2. The channel open probability values at 40 and −20 mV were typically 0.96 and 0.76, respectively. [b] Blocking kinetics for wild-type IbTX were published previously (*4*).

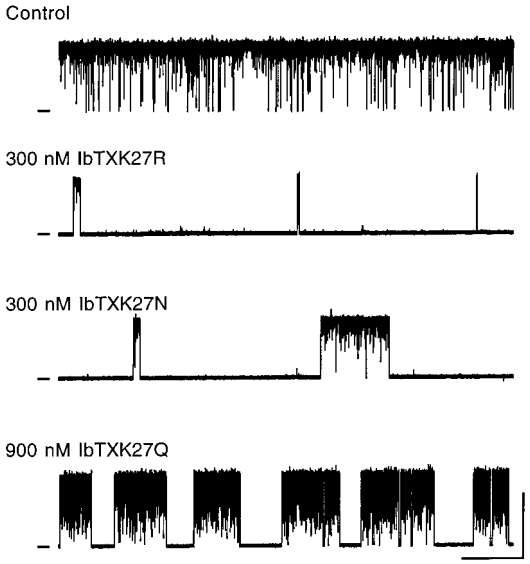

FIGURE 3: Effects of K27 mutations in IbTX on currents through single maxi-K channels. Currents through single maxi-K channels from bovine aortic smooth muscle incorporated into planar lipid bilayers are shown in the absence and presence of the IbTX mutants K27R, K27N, and K27Q. The closed current level is indicated by the lines to the left. The indicated time and current scale bars represent 30 s and 10 pA, respectively. Filtering and experimental conditions were as described in Figure 2.

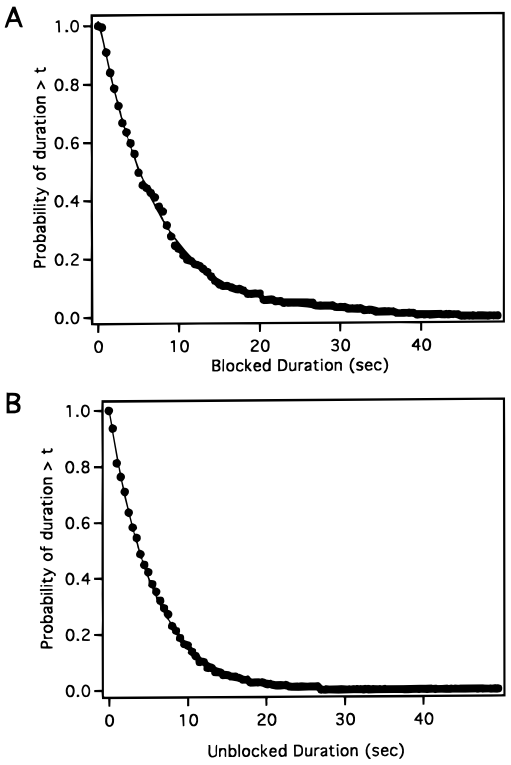

FIGURE 4: The durations of blocked and unblocked times in IbTX R34N are exponentially distributed. The durations of blocked (A) and unblocked (B) are plotted as cumulative dwell-time distributions in the presence of 900 nM IbTX R34N. The solid lines represent the best fit to a single exponential with time constants of 7 s for the blocked times and 5.5 s for the unblocked times. Distributions were constructed from 185 blocked events. Conditions were as described in Figure 2.

determinations, shown in Table 1, are 5-, 2-, 45-, and 40-fold shorter, respectively, than wild-type IbTX-blocked times. The large effects of R34N and K27Q on the toxin-blocked times suggests that these two residues form an important part of the IbTX−maxi-K channel interaction surface.

The simple bimolecular mechanism for toxin block of the maxi-K channel predicts that durations of toxin-blocked and -unblocked times be exponentially distributed (*4*). Figure 4 shows that, in the presence of 900 nM IbTXR34N, the toxin-blocked (part A) and -unblocked (part B) times are best described by single exponentials where the time constants for block and unblock were 7 and 5.5 s, respectively. Two other experiments were examined in a similar manner. Of these six dwell-time distributions for toxin block and unblock, none were best fit with two exponentials. These findings are consistent with a bimolecular mechanism, and they reveal that the fully cyclized IbTX R34N behaves as a single molecular species.

A more complete understanding of the effects of these mutations on specific IbTX binding with the maxi-K channel can be realized by examining the specific changes in binding free energy ($\Delta\Delta G_{bind}$) caused by these mutations. Figure 5 shows the specific changes in binding free energy caused by toxins mutated at positions K27 and R34. The changes in binding free energy caused by K27R, K27N, and K27Q were 0.83, 1.73, and 3.9 kcal/mol, respectively. While IbTX R34N and R34D caused changes in binding free energy of 3.45 and ≥5.4 kcal/mol, respectively. These changes in specific binding free energy from bilayer experiments are similar to relative changes in K_i values measured from inhibition of ^{125}I-ChTX binding to bovine aortic sarcolemmal membranes (see Materials and Methods). Therefore, the large changes in binding free energy observed for these mutations

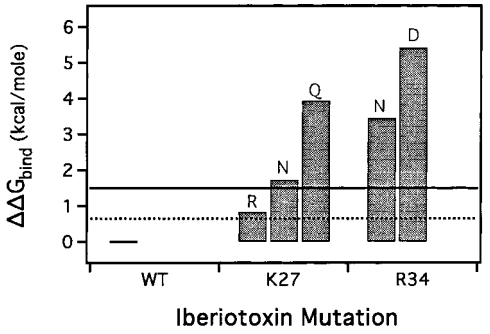

FIGURE 5: Mutations in K27 and R34 cause large, unfavorable changes in toxin binding free energy. Specific changes in binding free energy ($\Delta\Delta G_{bind}$) plotted for K27 and R34 mutations in IbTX were calculated from the ratio of the mutant to wild-type K_d values, $K_{d(mt)}$ and $K_{d(wt)}$, respectively, where $\Delta\Delta G_{bind} = RT \ln(K_{d(mt)}/K_{d(wt)})$. The dashed (0.646 kcal/mol) and solid (1.5 kcal/mol) lines plot energetic thresholds defining a residue as influential and critical parts of the binding surface, respectively (*2*, *12*).

further support that K27 and R34 in IbTX form part of the toxin−channel interaction surface.

K27 in IbTX Interacts with a Potassium Binding Site in the Maxi-K Channel Pore. Mechanistic studies with IbTX (*4*) and ChTX (*5*) have shown that the peptides electrostatically interact with a specific potassium binding site within the channel pore. The equilibrium occupancy of this K^+ site, and hence the toxin dissociation kinetics, can be modulated by either intracellular potassium or by membrane potential (*4*, *5*). Consequently, the toxin-blocked times increase as the membrane potential is hyperpolarized and K^+ ions are sucked out of their binding site in the pore.

To test whether K27 in IbTX also interacts with a K^+ site in the pore, we examined the effects of membrane potential on toxin-blocked times for the IbTX mutants K27R, K27N, K27Q, and R34N. Examination of toxin-blocked times in Table 1 shows that the blocked times for IbTXK27R are ~5-fold longer when the membrane potential is held at −20 mV compared to +40 mV while neutralization of K27 relieves the voltage dependence of block. In contrast, when R34 is neutralized to an asparagine, the toxin-blocked times increase ~1.7-fold over the same membrane potential range. This suggests that K27 in IbTX electrostatically interacts with a potassium binding site in the maxi-K channel pore. The effects of these electrostatic mutations on the voltage dependence of IbTX-blocking kinetics are qualitatively very similar to those obtained with analogous mutations in ChTX (*11*, *27*).

Neutralization of K27 and R34 Diminishes the IbTX Association Rate Constant. We have previously shown that IbTX-unblocked times decrease with increasing toxin concentration and thus are inversely related to the pseudo-first-order toxin association rate, k_{on}[toxin] (*4*). Inspection of single channel records for IbTX K27R and IbTX K27N in Figure 3 reveals that, at the same toxin concentration of 300 nM, the toxin-unblocked times for K27N are ~10-fold longer than those observed for K27R. This difference is quantitatively shown in Figure 6A by the distributions for IbTX K27R and IbTX K27N unblocked times. Both distributions were best fit by a single exponential, and the time constants for unblock were 1.7 and 13.3 s for IbTX K27R and IbTX K27N, respectively. Thus, for this experiment, the calculated k_{on} value for IbTX K27R (2×10^6 M^{-1} s^{-1}) is similar to

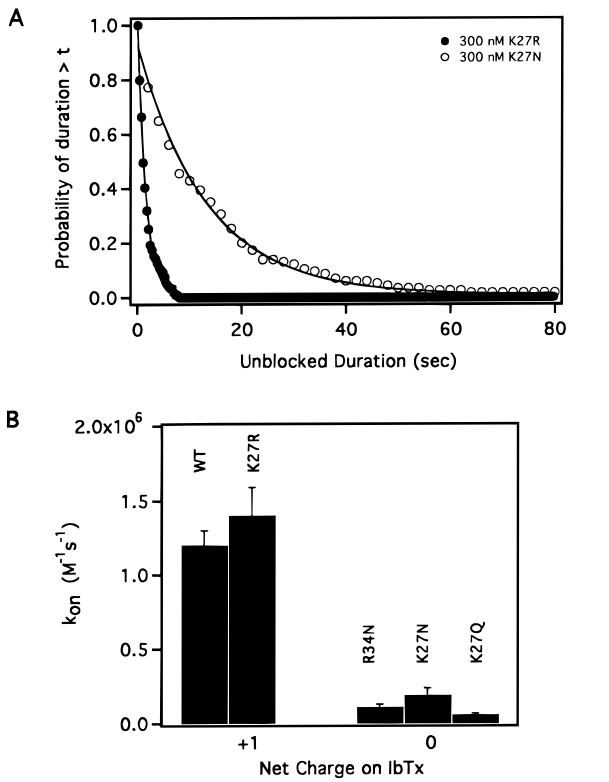

FIGURE 6: Charge neutralization in IbTX slows the toxin association rate constants. Part A plots durations of unblocked times in the presence of 300 nM K27R (●) and 300 nM K27N (○) as cumulative dwell-time distributions. The solid lines describe the best fit of the data to single exponentials with time constants for unblock of 1.7 and 13.3 s for K27R and K27N, respectively. Both distributions were constructed from >100 unblocked events. Part B plots the k_{on} values for wild-type IbTX and the mutants K27R, K27N, K27Q, and R34N averaged from two to nine separate experiments. Values for IbTX are from previously published work (*4*). Each value was obtained from a minimum of 35 blocking events. Conditions for wild-type and mutant toxins were similar and were as described in Figure 2.

that observed for wild-type IbTX (*4*) and is about 10-fold faster than the k_{on} value for IbTX K27N (2.5×10^5 M^{-1} s^{-1}). Figure 6B shows k_{on} values averaged from several experiments for wild-type IbTX and the mutants K27R, K27N, K27Q, and R34N as a function of toxin net charge. Similar to K27N, the average k_{on} values for K27Q and R34N were approximately 20- and 10-fold slower, respectively, relative to wild-type IbTX. Thus, neutralization of either K27 or R34 in IbTX causes significant diminution in the observed toxin association rate constant. This large effect of charge neutralization on toxin association rates is quite different from effects of similar mutations in ChTX (*11*).

These effects of charge neutralization suggest that the net charge on IbTX may control its rate of association with the channel. IbTX contains a net charge of +1; thus, neutralization of one basic residue in IbTX yields a species with no net charge. We have previously shown that the association rate constant values for wild-type IbTX decrease with increasing external potassium. However, according to simple Debye−Huckel (DH) theory, the k_{on} value for IbTX mutants with no net charge should not be influenced by external ionic strength. We recognize that K^+ is a "specific ligand" for the maxi-K channel. Consequently, we fully appreciate that, in these experiments, KCl does not provide a rigorous measure of ionic strength. However, we chose to vary KCl so that

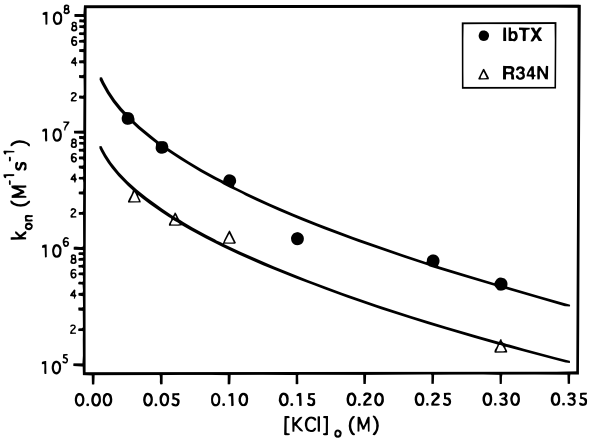

FIGURE 7: Effect of external potassium on the association rate constants for IbTX and for IbTXR34N. k_{on} values for wild-type IbTX (●), from previously published work (*4*), and for IbTX R34N (△), this work, are plotted as a function of external potassium concentration. Values for IbTX R34N were determined from two to five separate experiments and each value was obtained from a minimum of 35 blocking events. Values for wild-type IbTX were obtained from 22 independent experiments and analysis of 180 h of recording from a single channel. Conditions were as described in Figure 2 except that the concentration of extracellular potassium was varied from 30 to 300 mM and for IbTX R34N the membrane potential was 0 mV.

we could compare results from this work with our previously published data on IbTX (*4*). With this caveat in mind, we measured the k_{on} values for IbTX R34N as a function of external potassium. Figure 7 shows that the k_{on} values for IbTX and IbTX R34N are similarly influenced by external potassium. In addition, the k_{on} values for IbTX R34N are ~4-fold slower at all concentrations of external potassium. These slower k_{on} values for IbTX R34N are even observed at 300 mM KCl where long-range electrostatic interactions are minimal. These findings, which are unique to IbTX, suggest that simple net charge does not control the second-order association rate constant for IbTX.

DISCUSSION

Characteristics of the IbTX−Maxi-K Channel Interaction. In this study, we investigated the effects of electrostatic mutations in IbTX on its rates of binding and unbinding with the maxi-K channel outer vestibule. Previous studies showed that residues on the β-sheet face of another α-KTX, ChTX, interact with the maxi-K channel outer vestibule (*11, 12*). We thus focused on two basic residues, K27 and R34, which are located on the β-sheet face of IbTX and are highly conserved among the α-KTx's. All of the IbTX site-directed mutations at these two positions yielded specific changes in binding free energy that exceeded 1.5 kcal/mol excepting the conservative mutation K27R. Thus, our findings reveal that K27 and R34 are critical for IbTX binding to the maxi-K channel vestibule.

In this work, we have shown that the dissociation kinetics for IbTX K27R are enhanced by depolarizing membrane potentials. Previously, we showed that raising the concentration of internal potassium ions enhanced the IbTX dissociation kinetics (*4*). Together, these findings are consistent with a model where the stability of the IbTX−channel complex is regulated by the equilibrium occupancy of a voltage-dependent, K^+ binding site in the channel pore (*4*). Furthermore, we have shown that neutralization of K27 to either an asparagine or a glutamine alleviates these effects of voltage on the IbTX dissociation kinetics (Table 1). Collectively, our findings suggest that, similar to ChTX (*27*), K27 in IbTX electrostatically interacts with a voltage-dependent, potassium binding site in the maxi-K channel pore.

Specific Short-Range Electrostatic Interactions and the IbTX Association Rate. Neutralization of either K27 or R34 in IbTX caused an order of magnitude diminution in the toxin association rate constant relative to wild-type (Figure 6). This large decrease in toxin association rate has never been observed with ChTX, but similar effects were observed for LQ2 (α-KTx 1.2) when acidic residues on the *Shaker* potassium channel were neutralized (*28*). This large effect of charge neutralization on the toxin association rate constant suggests that ingress of IbTX to the channel may not be limited by diffusional processes. A nondiffusion-limited model was also proposed for LQ2 (*28*).

One caveat to this argument, however, is that electrostatic forces may influence the IbTX on-rate through Coulombic attraction. Electrostatic attraction that controls toxin association rates may result from Coulombic attraction that can extend over long ranges, i.e., >10 Å, where specific interactions between the toxin and channel cannot occur. If this is the case, then the effects we observe on the IbTX association rate would be entirely consistent with a diffusion-limited process.

Coulombic attraction arises from interactions between two point charges or monopoles. Debye−Huckel (DH) theory predicts that Coulombic attraction between the positively charged toxin and fixed negative charges on the channel will increase the local toxin concentration around the channel mouth to produce an apparently fast association rate constant. Increasing the ionic strength will attenuate this attraction and thus lower the observed association rate constant. Since IbTX contains a net positive charge of one, neutralization of R34 in IbTX produces a molecular species with no net charge. If we employ a grossly simple view, treating the toxin as a point sphere, then simple electrostatics predict that IbTX R34N should not be concentrated near the channel mouth. Thus, according to this simple view of DH theory, the k_{on} value for IbTX R34N should not depend on external ionic strength.

In this work we found that the association rate for IbTXR34N diminished ~19-fold as external potassium was increased from 30 to 300 mM. This behavior parallels the relationship we observed previously for wild-type IbTX (Figure 7). Since K^+ is a "specific ligand" for the maxi-K channel, KCl may not be a faithful reporter of ionic strength effects. However, we have previously reported that the association rate for wild-type IbTX was similarly influenced by external sodium and potassium (*4*). Thus, our findings show that long-range electrostatic forces arising from simple net charge on IbTX do not control its association rate. This finding is consistent with previous works on IbTX (*4*) and ChTX (*11*) suggesting that simple net charge on the toxin cannot completely account for the effects of external potassium on the toxin association rate.

The isopotential energy surfaces and molecular surfaces for IbTX, shown in Figure 1, are consistent with the observed effects of charge neutralization on IbTX association rates.

The positive isopotential surfaces around K27 and R34 are very close to the IbTX molecular surface. In this region, the distances between the molecular surface and the isopotential surfaces at 2 and 3 kT were ~ 4 and 2 Å, respectively. The surfaces we show were calculated with an ionic strength of 15 mM. However, when the same calculations were made at 150 mM ionic strength, the electrostatic and molecular surfaces were almost superimposable (not shown). The effects of charge neutralization on IbTX association rates we report in this work were observed at 150 mM external ionic strength (Figure 6). Thus, under our experimental conditions, these electrostatic isopotentials around IbTX do not extend beyond the molecular surface. Thus, these calculated isopotential and molecular surfaces suggest that interaction of IbTX with the maxi-K channel is controlled by short-range interactions which occur close (i.e., <4 Å) to the molecular surface.

Taken together, the isopotential surfaces around IbTX and our experimental data suggest that electrostatic potentials around IbTX are unlikely to have long-range effects in concentrating the toxin near the channel mouth. The question naturally arises, what types of electrostatic interactions could account for our experimental results? Examination of the isopotential surfaces around IbTX suggests two possible models that could account for the observed effects of charge neutralization on the IbTX association rate.

The first model uses dipolar interactions to explain the effects of charge neutralization on the IbTX association rate. The orientation and relative magnitude of the dipole moment for wild-type IbTX is shown in blue in Figure 1A. Although it is naive to describe peptide toxins as true dipoles, electrostatic theories predict that proteins with no net charge, but with a dipole moment, may display a significant ionic strength dependence in their association rates (*29*). However, the calculated dipole moments for IbTX (blue) and IbTX R34N (turquoise) appear quite similar in magnitude and relative orientation (Figure 1A). Consequently, in the absence of a high-resolution structure for the maxi-K channel vestibule, this limited view of toxin dipole moment provides no obvious explanation for the observed slower IbTX R34N association rate.

A second, physically more palatable model employs specific electrostatic interactions and a toxin-blocking mechanism that is not diffusion-limited. A simple model that might explain these effects involves a two-step reaction for IbTX block, as shown in Scheme 1. In the first step, IbTX forms an encounter complex (Tx--C), where the channel is not blocked. This reaction would include diffusional processes that involve random collisions between the toxin (Tx) and the channel (C). The second step, results in the formation of a bound complex (Tx:C) where no current can flow through the channel. In this second reaction, one could envision water molecules and cations being squeezed out of the vestibule to form a tightly bound toxin:channel complex.

Scheme 1

$$\mathrm{Tx} + \mathrm{C} \rightleftharpoons \mathrm{Tx{-}{-}C} \rightleftharpoons \mathrm{Tx{:}C}$$

The proximity between toxin and channel in Tx:C would allow electrostatic repulsion between specific basic residues on the toxin and monovalent cations in the channel vestibule. Positive isopotentials originating from basic residues on the toxin β-sheet face would repel cations from their sites in the vestibule. This simple model could also account for the slower association rate constants we observe for the charge neutralized IbTX mutants, K27 and R34. Neutralization of these basic residues significantly reduces the positive isopotential around the β-sheet face (not shown). Thus, neutralization of K27 and R34 would decrease the ability of IbTX to repel cations from the vestibule. This model employs specific, short-range interactions between basic residues on the toxin β-sheet face and cationic sites in the channel vestibule to account for the effects of charge neutralization on the IbTX association rate.

The experiments presented in this work do not allow rigorous distinction between the influence of toxin dipole moment and specific, short-range interactions on the IbTX association rate. Naively, the toxin dipole moment could modulate the IbTX association rate by facilitating a favorable orientation between the toxin and channel. In contrast, specific interactions could modulate the IbTX association rate via electrostatic repulsion between basic toxin residues and monovalent cations in the channel. These two possibilities could be differentiated by careful examination of ionic strength effects on toxin association rate. The latter model, however, is functionally more interesting since it may provide a means for probing specific cationic sites in the maxi-K channel vestibule which underlie permeation. If such specific, short-range interactions are at work, then the electrostatic structure of IbTX may provide a unique view into the structures that underlie maxi-K channel function.

ACKNOWLEDGMENT

We thank Dr. Marilyn Gunner (City College of New York) for valuable discussions and suggestions with regard to protein electrostatics. We are grateful to Dr. Valerie Fremont for critical comments on the manuscript.

REFERENCES

1. Garcia, M. L., Hanner, M., Knaus, H.-G., Koch, R., Schmalhofer, W., Slaughter, R. S., and Kaczorowski, G. J. (1997) *Adv. Pharmacol. 39*, 425−471.
2. Giangiacomo, K. M., Gabriel, J., Fremont, V., and Mullmann, T. J. (1999) in *Perspectives in Drug Discovery and Design* (Darbon, H., and Sabatier, J.-M., Eds.) Kluwer Academic Publishers, Dordrecht, The Netherlands.
3. Miller, C. (1995) *Neuron 15*, 5−10.
4. Giangiacomo, K. M., Garcia, M. L., and McManus, O. B. (1992) *Biochemistry 31*, 6719−6727.
5. MacKinnon, R., and Miller, C. (1988) *J. Gen. Physiol. 91*, 335−349.
6. Miller, C. (1988) *Neuron. 1*, 1003−1006.
7. Goldstein, S. A. N., and Miller, C. (1993) *Biophys. J. 65*, 1613−1619.
8. MacKinnon, R., Heginbotham, L., and Abramson, T. (1990) *Neuron 5*, 767−771.
9. MacKinnon, R., and Yellen, G. (1990) *Science 250*, 276−279.
10. Yellen, G., Jurman, M. E., Abramson, T., and MacKinnon, R. (1991) *Science 251*, 939−942.
11. Park, C. S., and Miller, C. (1992) *Biochemistry 31*, 7749−7755.
12. Stampe, P., Kolmakova-Partensky, L., and Miller, C. (1994) *Biochemistry 33*, 443−450.
13. Gross, A., and MacKinnon, R. (1996) *Neuron 16*, 399−406.
14. Goldstein, S. A. N., Pheasant, D. J., and Miller, C. (1994) *Neuron. 12*, 1377−1388.

15. Jordan, P. C. (1987) *Biophys. J. 51*, 297−311.
16. Galvez, A., Gimenez-Gallego, G., Reuben, J. P., Roy-Contancin, L., Feigenbaum, P., Kaczorowski, G. J., and Garcia, M. L. (1990) *J. Biol. Chem. 265*, 11083−11090.
17. Koschak, A., Koch, R. O., Liu, J., Kaczorowski, G. J., Reinhart, P. H., Garcia, M. L., and Knaus, H.-G. (1997) *Biochemistry 36*, 1943−1952.
18. Novick, J., Leonard, R. J., King, V. F., Schmalhofer, W., Kaczorowski, G. J., and Garcia, M. L. (1991) *Biophys. J. 59*, 78a.
19. Ranganathan, R., Lewis, J. H., and MacKinnon, R. (1996) *Neuron 16*, 131−139.
20. Hidalgo, P., and MacKinnon, R. (1995) *Science 268*, 307−310.
21. Slaughter, R. S., Shevell, J. L., Felix, J. P., Garcia, M. L., and Kaczorowski, G. J. (1989) *Biochemistry 28*, 3995−4002.
22. Knaus, H.-G., Schwarzer, C., Koch, R. O. A., Eberhart, A., Kaczorowski, G. J., Glossmann, H., Wunder, F., Pongs, O., Garcia, M. L., and Sperk, G. (1996) *J. Neurosci. 16*, 955−963.
23. Garcia-Calvo, M., Leonard, R. J., Novick, J., Stevens, S. P., Schmalhofer, W., Kaczorowski, G. J., and Garcia, M. L. (1993) *J. Biol. Chem. 268*, 18866−18874.
24. Johnson, B. A., and Sugg, E. E. (1992) *Biochemistry 31*, 8151−8159.
25. Gunner, M. R., and Honig, B. (1991) *Proc. Natl. Acad. Sci. U.S.A. 88*, 9151−9155.
26. Nicholls, A., Sharp, K. A., and Honig, B. (1991) *Proteins 11*, 281−296.
27. Park, C. S., and Miller, C. (1992) *Neuron 9*, 307−313.
28. Escobar, L., Root, M. J., and MacKinnon, R. (1993) *Biochemistry 32*, 6982−6987.
29. Koppenol, W. H. (1980) *Biophys. J. 29*, 493−508.

BI982040+